Pharmacogn. Mag.
A multifaceted peer reviewed journal in the field of Pharmacognosy and Natural Products
www.phcog.com | www.phcog.net

ORIGINAL ARTICLE

Phenolics from the Heartwood of *Tecoma mollis* as Potential Inhibitors of COVID-19 Virus Main Protease and Spike Proteins: An *In silico* Study

Lamya H. Al-Wahaibi, Md Tabish Rehman[1], Muneera S. M. Al-Saleem, Omer A. Basudan[1], Ali A. El-Gamal[1], Mohamed F. AlAjmi[1], Enaam Y. Backheet[2], Azza A. Khalifa[2], Wael Mostafa Abdel-Mageed[1,2]

Department of Chemistry, Science College, Princess Nourah Bint Abdulrahman University, [1]Department of Pharmacognosy, College of Pharmacy, King Saud University, Riyadh, Saudi Arabia, [2]Department of Pharmacognosy, Faculty of Pharmacy, Assiut University, Assiut, Egypt

Submitted: 19-Jan-2021 Revised: 02-Jun-2021 Accepted: 26-Jul-2021 Published: 15-Sep-2021

ABSTRACT

Background: The severe acute respiratory syndrome coronavirus 2 (SARS-CoV-2) is an emerging novel coronavirus responsible for the viral pneumonia outbreak (coronavirus disease-19 [COVID-19]) that has impacted millions of people, causing a tremendous global public health concern and number of fatalities. The development of novel antiviral agents is considered an urgent research subject. **Objectives:** The objective of the study is to discover the phenolic constituents of the methanolic extract of *Tecoma mollis* Humb. and Bonpl. heartwood and to investigate their potential inhibitory action against SARS-CoV-2 protease and/or entry proteins. **Materials and Methods:** The heartwood of *T. mollis* was extracted by maceration with 70% EtOH until complete exhaustion. The extract was concentrated under reduced pressure, mixed with distilled H_2O and defatted with $CHCl_3$ to produce a $CHCl_3$ fraction, and then subjected to solvent fractionation with *n*-butanol to produce an *n*-butanol fraction. The *n*-butanol fraction was subjected to a silica gel column using $CHCl_3$–MeOH gradient mixtures followed by reversed-phase high-performance liquid chromatography. The isolated compounds were identified using one- and two-dimensional nuclear magnetic resonance as well as mass spectroscopy. Molecular docking studies have been implemented to identify the binding pattern between ligands and target enzymes, i.e. main protease (M^{pro}) and spike protein receptor-binding domain (RBD), and compared with the currently used COVID-19 inhibitors. Molecular dynamic simulations have been performed to evaluate the dynamics and stability of protein–ligand complexes. The obtained information is then correlated with the essential structural features, and finally the structure–activity relationship is suggested. **Results:** Fourteen phenolic glycosides were isolated from the methanolic extract of *T. mollis* Humb. and Bonpl. heartwood in addition to an iridoid, ixoside. The molecular docking study exhibited that the isolated compounds have a higher binding affinity toward the active site of M^{pro} and the angiotensin-converting enzyme-2 binding site of spike protein RBD. The phenylpropanoids have higher inhibitory action with higher binding energy toward SARS-CoV-2 M^{pro} protease as compared to spike protein RBD. Among all the isolated compounds, isoverbascoside (10) exhibited the most potent dual interaction with SARS-CoV-2 M^{pro} protease and spike protein RBD with high binding energy of – 8.8 and – 7.2 kcal/mol, respectively. This showed better potency than the currently used M^{pro} and spike–protein inhibitors. **Conclusion:** Our study is the first report on the potential inhibitory action of phenylpropanoids for SARS-CoV-2 protease and spike protein. It also correlates between the reported antiviral activities of some isolated compounds with their potential inhibitory action for COVID-19 viral proteins. Our results on *T. mollis* extract constituents could help in the discovery of a promising repurposable drug candidate that could contribute to the development of an effective therapy for COVID-19.

Key words: *In silico* study, isoverbascoside, phenylpropanoids, protease inhibition, severe acute respiratory syndrome coronavirus 2, spike protein, *Tecoma mollis*

SUMMARY

- Phytochemical investigation of *Tecoma mollis* heartwood yielded 15 compounds
- The phenylpropanoids have more inhibitory action to severe acute respiratory syndrome coronavirus 2 (SARS-CoV-2) protease than spike protein
- Isoverbascoside exhibited the most potent interaction with SARS-CoV-2 main protease and spike protein.

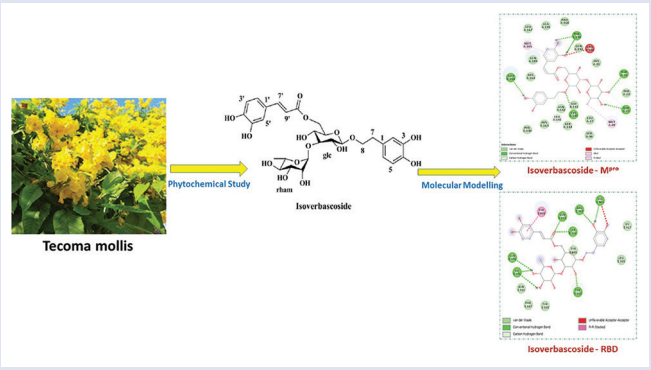

Abbreviations used: SARS-CoV-2: Severe acute respiratory syndrome coronavirus 2; COVID-19: Coronavirus disease-19; S-protein: Spike protein; ACE2: Angiotensin-converting enzyme-2; M^{pro}: Main protease; CC: Column chromatography; NMR: Nuclear magnetic resonance; TLC: Thin layer chromatography; RP: Reversed phase; UV: Ultraviolet; HPLC: High-performance liquid chromatography; RBD: Receptor-binding domain; MMFF: Merck molecular force field; Tyr: Tyrosine; Glu: Glutamic acid; Cys: Cysteine; Met: Methionine; Gly: Glycine; Val: Valine; Thr: Threonine; Ser: Serine; Phe: Phenylalanine; Pro: Proline; Leu: Leucine; Ala: Alanine; Asn: Asparagine; Ala: Alanine; His: Histidine; Arg: Arginine; Gln: Glutamine; Trp: Tryptophan; SAR: Structural activity relationship.

Correspondence:

Dr. Wael Mostafa Abdel-Mageed,
Department of Pharmacognosy, College of Pharmacy, King Saud University, P.O. Box 2457, Riyadh 11451, Saudi Arabia.
Department of Pharmacognosy, Faculty of Pharmacy, Assiut University, Assiut 71526, Egypt.
E-mail: wabdelmageed@ksu.edu.sa

DOI: 10.4103/pm.pm_35_21

Access this article online
Website: www.phcog.com
Quick Response Code:

Cite this article as: Al-Wahaibi LH, Rehman MT, Al-Saleem MS, Basudan OA, El-Gamal AA, AlAjmi MF, *et al*. Phenolics from the heartwood of *Tecoma mollis* as potential inhibitors of COVID-19 virus main protease and spike proteins: An *in silico* study. Phcog Mag 2021;17:S278-86.

INTRODUCTION

Severe acute respiratory syndrome coronavirus 2 (SARS-CoV-2) is the leading cause of the global viral pneumonia outbreak, namely coronavirus disease-19 (COVID-19). SARS-CoV-2 is an enveloped, positive-sense, single-strand RNA virus, which etiologically belongs to the coronaviruses (order *Nidovirales*, family *Coronaviridae*, subfamily *Orthocoronavirinae*, genus *Betacoronavirus*). The main target of SARS-CoV-2 is the respiratory system of humans.[1,2] The clinical symptoms of COVID-19 vary greatly, ranging from asymptomatic carrying to severe pneumonia, acute respiratory distress syndrome, acute lung injury, multiple organ failure, and death.[1,2] The coronaviruses comprise four structural proteins, i.e. spike glycoprotein (S-protein), membrane glycoproteins, envelope protein, and nucleocapsid proteins.[3] The S-protein is considered the most crucial protein that promotes the process of viral attachment and penetration of the host cell. The S-protein assists the viral entrance to host cells through its capability to bind with the host protein angiotensin-converting enzyme-2 (ACE2), which serves as SARS-CoV-2 entry receptor.[4,5] Thus, impeding viral entrance through the disruption of spike protein–ACE2 connection can be considered a crucial tactic for the development of medical treatment of COVID-19 infection.

The other suggested therapies that could be suitable options for medical treatments are using ACE2 receptor antagonists to block coronavirus–host interactions; RNA-dependent RNA polymerase inhibitors, such as remdesivir; RNA metabolism interference such as ribavirin; agents that disrupt intracellular trafficking and viral fusion events such as chloroquine and its derivatives hydroxychloroquine; immunotherapeutic agents and vaccines; and finally, the main protease (M^{pro}) inhibitors such as darunavir, lopinavir, and ritonavir.[6] Furthermore, the published high-resolution structures of COVID-19 protease (M^{pro}) and S-protein created excellent opportunities for the development of both protease and/or S-protein inhibitors as a pivotal tool for controlling viral transcription, replication, as well as viral entrance to the host cell.[7,8]

To date, no specific medication is available for COVID-19, although several protocols of drug repurposing were tested and some of them are currently in clinical trials.[9] Thus, discovering and/or designing new drugs is an essential and critical way to overcome this global crisis. In this regard, *in silico* drug discovery and designing methods are considered as cost-efficient and time-saving. The *in silico* approach has a remarkable role to play as a quick technique for the drug discovery as compared to experimental studies using trial-and-error methods.

Plants are a prolific source of structurally-unique and chemically-diverse natural products that act as a valuable source for drug leads. Herbal plants provide a wide variety of alternative and integral treatments that may address issues with many viral diseases. According to the World Health Organization (WHO), about 80% of humans in developing nations depend on traditional plants for health requirements. Thus, natural plant products have received great attention from researchers aiming to discover a potential drug to treat COVID-19 and assist in solving this global crisis.

One such plant, *Tecoma mollis* Humb. and Bonpl. (family *Bignoniaceae*), is an ornamental plant, which ranges from the size of an upright shrub to that of a large tree. The plant is native to South America, Argentina, Venezuela, and Mexico and holds economic significance as an ornamental lumber plant.[10-13] The plant's phytochemical study reported the presence of phenylpropanoids, iridoids, flavonoids, alkaloids, and triterpenes.[10-13] Many biological activities of *T. mollis* such as antiprotozoal, anti-inflammatory, hypoglycemic, antioxidant, antimicrobial, and antiproliferative activities have been reported.[10-13] Interestingly, it had been reported that phenylpropanoids and iridoids, the main active constituents, possess antiviral activity toward different viruses such as respiratory syncytial virus (RSV), vesicular stomatitis virus (VSV), and influenza virus.[14-16]

The current study was designed to isolate the chemical constituents of the heartwood of *T. mollis* and evaluate their virtual efficacy against COVID-19 protease and spike protein using molecular docking and molecular dynamic simulation studies. The binding affinity of the identified compounds was additionally compared with the reported protease inhibitors, such as ritonavir, darunavir, and lopinavir, as well as spike protein inhibitors, such as azithromycin.[6,17-20]

MATERIALS AND METHODS

General

High-performance liquid chromatography (HPLC) was carried out using Shimadzu HPLC-LC-20 AD series binary gradient pump with Shimadzu SPD-M20A detector (Tokyo, Japan) on Phenomenex reversed-phase (RP) column (Jupiter Proteo 90 Å, 250 mm × 10 mm, 4 μm). Column chromatography (CC) was performed using a silica gel (Kiesel gel 60 Å, 40–63 μM mesh size, Fluorochem, UK). The thin layer chromatography (TLC) analysis was done using RP-18 F_{254S} (Merck) and Kiesel gel 60 F_{254} plates. Compounds were detected at 254 nm using an ultraviolet (UV) lamp (Entela Model UVGL-25) and sprayed by *p*-anisaldehyde/H_2SO_4 reagent. Nuclear magnetic resonance (NMR) experiments were measured on UltraShield Plus 500 MHz (Bruker). UV absorption was carried out using a UV-visible spectrometer (Cary 50 spectrophotometer). Molecular docking study was performed on HP Windows Laptop, 2.5 GHz Intel Core i5 with 8 GB RAM using Autodock-Vina.[21] Molecular interactions between ligands and target proteins were analyzed using Discovery Studio 2020 (BIOVIA).[22] Molecular dynamics were performed on Intel Xenon workstation-E3-1245-8C, 3.50 GHz processor with 28 GB RAM. The workstation was powered by a NVIDIA Quadro P5000 GPU card.

Plant material

The heartwood of *T. mollis* was collected from the trees cultivated in the Faculty of Agriculture's Experimental Station, Assiut University, Egypt, in July 2015. The plant was kindly identified by Prof. Gamal Taha, Department of Horticulture, Faculty of Agriculture, Assiut University, Egypt. A voucher specimen (no. 2015TM) was deposited at the Pharmacognosy Department, Faculty of Pharmacy, Assiut University, Egypt.

Extraction and isolation of the plant compounds

450 g of the air-dried powdered heartwood was extracted by maceration with 70% EtOH until complete exhaustion (3 L × 3) to provide an ethanolic extract (56.7 g, 12.6%). The extract was concentrated under reduced pressure and then mixed with 750 mL of distilled H_2O and defatted with $CHCl_3$ to produce a $CHCl_3$ fraction (17.2 g). The aqueous fraction was subjected to solvent fractionation with *n*-butanol and then concentrated under reduced pressure to produce an *n*-butanol fraction (28.1 g). This fraction was subjected to a silica gel column using $CHCl_3$–MeOH gradient mixtures.

A total of 131 fractions (100 mL each) were collected and monitored on TLC to combine similar fractions yielding 14 groups. The groups were subsequently purified using RP HPLC Phenomenex (Jupiter Proteo 90 Å, 250 mm × 10 mm, 4 μm) column and a gradient of 5%–100% CH_3CN–H_2O over 40 min. Group **5** (fractions 42–51) afforded compounds **1** (26.3 mg), **2** (10.7 mg), and **10** (12.9 mg); group **6** (fractions 52–64)

afforded compounds **12** (5.4 mg), **13** (7.1 mg), and **14** (13.6 mg); group **8** (fractions 70–80) afforded compounds **3** (18.4 mg), **4** (7.1 mg), and **11** (15.5 mg); group **9** (fractions 81–94) afforded compounds **5** (4.4 mg), **6** (6.1 mg), and **7** (9.5 mg); group **10** (fractions 95–101) afforded compounds **8** (5.1 mg) and **9** (13.2 mg); and finally, the purification of group **11** (fractions 102–108) afforded compound **15** (3.4 mg).

Docking studies

The molecular interaction between *T. mollis* compounds and the target molecules (i.e. the M^{pro} of SARS-CoV-2 and receptor-binding domain [RBD] of the S-protein) was performed using AutoDock4.2 as described earlier.[23] The two-dimensional (2D) structures of compounds were drawn in ChemSketch, and their energies were minimized using universal force filed before docking. The 3D coordinates of M^{pro} (protein databank [PDB] ID: 6 LU7) and RBD (PDB ID: 6M0J) were downloaded from the Research Collaboratory for Structural Bioinformatics PDB. The structure of proteins was preprocessed by deleting noncatalytic water molecules and any other heterogeneous molecule. Missing hydrogen atoms were added, and a network of hydrogen bonds was created. The complete system was energy-minimized using Merck molecular force field.[24]

For M^{pro}, molecular docking was performed inside a grid-box of 18 Å ×24 Å ×19 Å dimensions placed at − 11.2, 14.9, and 68.9 Å with 0.375 Å spacing, while the molecular docking against RBD was performed using a grid box of 26 Å ×45 Å ×24 Å dimensions centered at − 38.6, 29.6, and 4.1 Å with 0.375 Å spacing, with the engagement of Lamarckian genetic algorithm along with Solis and Wets local search methods.[25] The initial positions of compounds, their orientation, and torsions were fixed arbitrarily. For each docking run, a maximum of 2,500,000 energy calculations were computed with population size, translational step, torsion steps, and quaternions set at 150, 0.2 Å, 5 and 5, respectively. The results were analyzed and figures were prepared in Discovery Studio (Accelrys). The docking affinity (K_d) of the compounds toward M^{pro} was evaluated from docking energy (ΔG) using the below equation: [26]

$$\Delta G = - RT \ln K_d$$

where R and T were Boltzmann gas constant and temperature.

Molecular dynamics simulation studies

MD simulation of target proteins (M^{pro} and spike protein RBD) with the corresponding ligands, namely ritonavir, azithromycin, and isoverbascoside, was performed using "Desmond (Schrodinger-2020, LLC, NY, USA)" as described earlier.[23,24] Briefly, an orthorhombic box was selected for the MD simulation by placing the protein–ligand complex at the center, with at least 10 Å away from the box. The simulation box was solvated with TIP3P water molecules and neutralized by adding proper counter ions. Salt (150 mM NaCl) was added to mimic the physiological conditions. An iteration of 1000 steps with convergence criteria of 1 kcal/mol/Å was performed to minimize the energy of the system using OPLS3e force field. An MD simulation run of 100 ns was performed under NPT ensemble at 298 K and 1 bar. Nose-Hoover Chain thermostat and Matrtyna-Tobias-Klein barostate were employed to maintain the temperature and pressure of the system.[27,28] A time step of 2 fs was fixed, and energies and structures were recorded at every 10 ps in the trajectory. The parameters such as root mean square deviation (RMSD), root mean square fluctuation (RMSF), radius of gyration (Rg), solvent accessible surface area (SASA), secondary structure analysis, and total number of contacts formed between protein and ligand were analyzed to establish the stability of protein–ligand complexes.

RESULTS AND DISCUSSION

Structure elucidation of the isolated compounds

Based on the physiochemical and spectral data using UV, 1D and 2D NMR, and mass spectroscopy (MS) and chromatographic properties and by comparing with the literature and reported data, 15 compounds were identified as verbascoside (**1**), 6'-*O*-acetyl verbascoside (**2**), luteoside A (**3**), 2'-*O*-β-apiosyl verbascoside (**4**), tecomolliside A (**5**), tecomolliside B (**6**), myricoside (**7**), tecomoloside (**8**), crassoside (**9**), isoverbascoside (**10**), luteoside B (**11**), seguinoside L (**12**), seguinoside K (**13**), 1-(α-L-rhamnosyl-(1 → 6)-O-β-D-glucopyranosyloxy)-3,4,5-tri methoxybenzene (**14**), and ixoside (**15**) [Figure 1, Supplementary Figure 1 and Tables 1-3]. This was the first time the compounds were isolated from the heartwood of *T. mollis*, although they were previously isolated from other organs (i.e. root and stem bark) of *T. mollis*.[12,13]

Anti-severe acute respiratory syndrome coronavirus 2 molecular docking study

Docking to severe acute respiratory syndrome coronavirus 2 main protease

The first X-ray crystal structure of SARS-CoV-2 M^{pro} in complex with the N3 inhibitor was reported by Jin *et al*.[29] M^{pro} comprises 306 amino acid residues folded into three different domains I–III. Domain I consists of amino acid residues 8–101, while domain II comprises amino acid residues 102–184 and they have an antiparallel beta structure. The amino acid residues 201–303 forming domain III comprises five α-helices organized into an antiparallel globular cluster. Doman III is connected to domain II through a loop region spanning amino acid residues 185–200. A deep cleft between domains I and II harbors substrate-binding site of M^{pro} lined with a Cys^{41}-His^{145} catalytic dyad.

In this study, the 3D coordinates of M^{pro} were used as template to screen the binding affinity of compounds isolated from *T. mollis*. The relative binding of bioactive compounds to the M^{pro} substrate-binding site is described in Table 1. The detail of the protein–ligand interaction is presented in Supplementary Figure 2 and Supplementary Table 4. It is clear that all the bioactive compounds from *T. mollis* have a docking energy in the range of − 7.3 to − 8.8 kcal/mol [Table 1]. The lowest binding energy was exhibited by isoverbascoside (**10**), and hence, it was further used for detailed analysis. The analysis of the M^{pro} – TM10 interaction revealed that TM10 formed two carbon–hydrogen bonds with Thr^{25} and Leu^{141}, in addition to two hydrophobic interactions with Met49 and Met165. In addition, TM10 formed eight conventional hydrogen bonds with Thr^{25}, Thr^{26}, active site residue Cys^{145}, Glu^{166}, and Thr^{190} to stabilize the Mpro-TM10 complex [Table 1 and Figure 2b]. Moreover, TM-10 also formed a network of van der Waals' interaction with Thr^{24}, Leu^{27}, His^{41}, Ser^{46}, Phe^{140}, Asn^{142}, Gly^{143}, Ser^{144}, His^{163}, His^{164}, Leu^{167}, Pro^{168}, Gln^{189}, Ala^{191}, and Gln^{192}. The docking energy and binding affinity of TM-10 toward M^{pro} were estimated to be − 8.8 kcal/mol and 2.85×10^6 M^{-1}, respectively.

The analysis of the interaction between M^{pro} and other *T. mollis* compounds shows considerably good binding affinities for all compounds. All the compounds have been shown to bind the substrate-binding site of M^{pro} and potentially interact with the key active site residues of the enzyme. All the compounds, except TM-07 and TM-12, interacted with the catalytic residue Cys^{145}, while TM-05, TM-07, TM-08, TM-09, and TM-12 interacted with another catalytic residue, i.e. His^{41}. The interaction of *T. mollis* compounds and Cys^{145} was mediated primarily through hydrogen bond(s), except TM-02, which formed hydrophobic interaction with Cys^{145}. Similarly, TM-05, TM-07, TM-08, and TM-11 interacted electrostatically with His^{41}, while TM-09 formed a hydrogen

Table 1: Molecular docking parameters for the interaction of compounds from *Tecoma mollis* with the main protease (main protease) of severe acute respiratory syndrome coronavirus 2

Compound	ΔG kcal mol^{-1}	Receptor amino acid
TM-01	−8.4	Leu^{141}, Ser^{144}, Cys^{145}, Glu^{166}, Gln^{189}, Thr^{190}, His^{163}, Met^{165}, His^{172}
TM-02	−8.4	Met^{165}, Arg^{188}, Met^{49}, Gly^{143}, His^{163}, Thr^{190}, Leu^{27}, Cys^{145}
TM-03	−7.6	Gln^{189}, Met^{49}, Thr^{24}, Leu^{141}, Gly^{143}, Ser^{144}, Cys^{145}, Met^{165}, Thr^{190}
TM-04	−8.3	Thr^{45}, Gln^{189}, Met^{49}, Thr^{25}, Cys^{44}, Leu^{141}, Gly^{143}, Cys^{145}, His^{163}, Arg^{188}, Gln^{189}, Thr^{190}, Met^{165}
TM-05	−8.2	Thr^{24}, Asn^{142}, Gln^{189}, His^{41}, Met^{165}, Cys^{44}, Thr^{45}, Ser^{46}, Thr^{190}, Met^{49}, Cys^{145}
TM-06	−8.3	Thr^{26}, Met^{165}, Thr^{25}, Thr^{45}, Ser^{46}, Met^{49}, Cys^{145}, Thr^{190}
TM-07	−8.2	His^{41}, Met^{49}, Met^{165}, Thr^{25}, Thr^{45}, Ser^{46}, Arg^{188}, Thr^{190}
TM-08	−8.4	His^{41}, Met^{49}, Asn^{142}, Met^{165}, Thr^{26}, Cys^{145}, Thr^{190}
TM-09	−8.4	Thr^{25}, Gln^{189}, Met^{165}, Met^{49}, Thr^{24}, Thr^{26}, His^{41}, Leu^{141}, Gly^{143}, Ser^{144}, Cys^{145}
TM-10	−8.8	Thr^{25}, Leu^{141}, Met^{49}, Met^{165}, Thr^{26}, Cys^{145}, Glu^{166}, Thr^{190}
TM-11	−8.0	Met^{49}, Met^{165}, Cys^{145}, Thr^{190}
TM-12	−8.3	Met^{165}, His^{41}, Glu^{166}, Leu^{141}, Asn^{142}, Arg^{188}, Thr^{190}, Met^{49}, Pro^{168}
TM-13	−7.9	Met^{165}, Cys^{145}, Met^{49}, Gln^{189}, Thr^{190}, Ser^{144}, His^{164}
TM-14	−7.5	Arg^{188}, Met^{49}, Met^{165}, Thr^{26}, Leu^{141}, Asn^{142}, Ser^{144}, Cys^{145}
TM-15	−7.3	Asn^{142}, Cys^{145}, His^{163}, Glu^{166}, Met^{165}
Darunavir	−8.0	Glu^{166}, Met^{165}, His^{164}, Cys^{145}, Leu^{141}, His^{41}, Leu^{27}, Thr^{24}
Lopinavir	−8.1	Pro^{168}, Glu^{166}, Cys^{145}, Met^{49}, His^{41}
Remdesivir	−7.8	Met^{165}, Cys^{145}, Asn^{142}, Leu^{141}, Met^{49}, His^{41}
Ritonavir	−8.3	Ala^{191} Gln^{189}, Glu^{166}, Pro^{168}, Met^{165}, Cys^{145}, Asn^{142}, Leu^{141}, Phe^{140}, Met^{49}, His^{41}

Leu: Leucine; Ser: Serine; Glu: Glutamic acid; Cys: Cysteine; Thr: Threonine; Gln: Glutamine; His: Histidine; Met: Methionine; Arg: Arginine; Gly: Glycine; Ala: Alanine; Asn: Asparagine; Phe: Phenylalanine; Pro: Proline; TM: *Tecoma mollis*

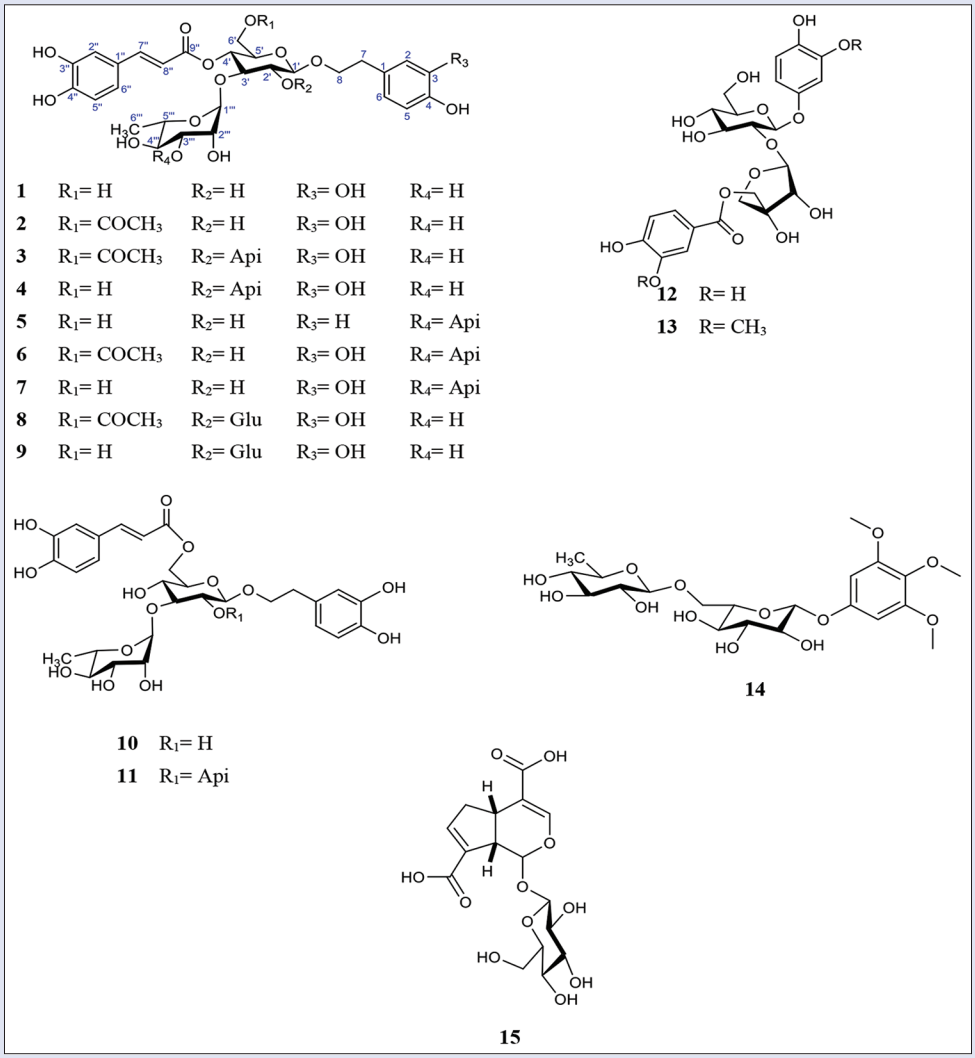

Figure 1: Structure of the isolated compounds (**1**–**15**) (Glu: β-D-glucopyranosyl, Api: β-D-apiofuranosyl)

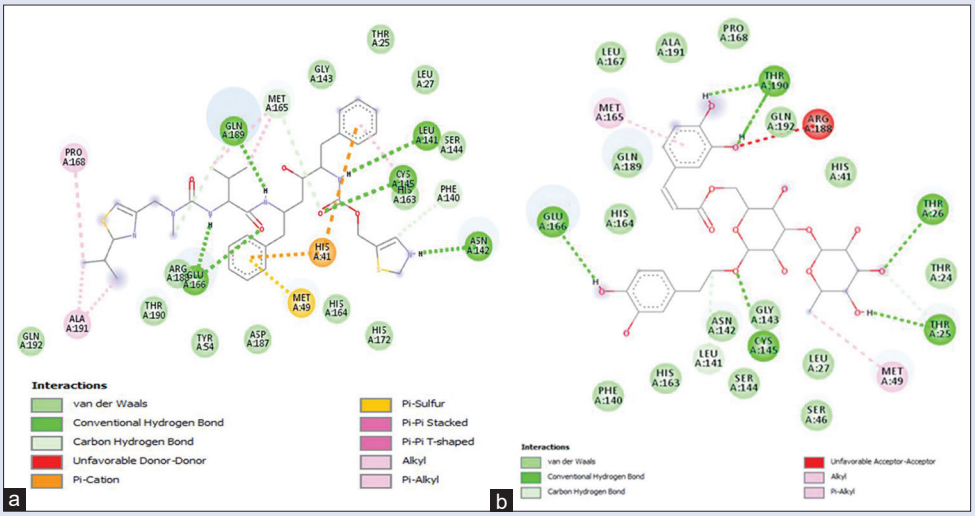

Figure 2: Two-dimensional ligand interaction diagram of (a) ritonavir and (b) isoverbascoside, with the main protease (M^{pro}) of severe acute respiratory syndrome coronavirus 2. Tyr: Tyrosine; Glu: Glutamic acid; Cys: Cysteine; Met: Methionine; Gly: Glycine; Val: Valine; Thr: Threonine; Ser: Serine; Phe: Phenylalanine; Pro: Proline; Leu: Leucine; Ala: Alanine; Asn: Asparagine; Ala: Alanine; His: Histidine; Arg: Arginine; Gln: Glutamine; Trp: Tryptophan

bond. Thus, compounds isolated from *T. mollis* could be developed as effective inhibitors of the SARS-CoV-2 M^{pro}.

To strengthen our finding, we performed docking of ritonavir (a control inhibitor of M^{pro}) to the active site of M^{pro} and the results are presented in Table 1, Figure 2a, and Supplementary Table 5 and Supplementary Figure 3 and Table 5. The M^{pro}–ritonavir complex was stabilized by six conventional hydrogen bonds (Leu^{141}, Asn^{142}, Cys^{145}, Glu^{166}, and Gln^{189}) and three carbon–hydrogen bond (Phe^{140}, Met^{165}, and Gln^{189}). In addition, the active site residue His^{41} formed two electrostatic interactions and two hydrophobic interactions with ritonavir. Furthermore, several other residues such as Met^{165}, Pro^{168}, and Ala^{191} and another active site residue Cys^{145} formed six additional hydrophobic interactions. The SD group of Met^{49} was engaged in a Pi–sulfur interaction with ritonavir. The M^{pro}–ritonavir complex was further stabilized by van der Waals' interactions with Thr^{25}, Leu^{27}, Tyr^{54}, Gly^{143}, Ser^{144}, His^{164}, His^{172}, Arg^{186}, Asp^{187}, Thr^{190}, and Gln^{192} [Figure 2a]. The docking energy and binding affinity of ritonavir toward M^{pro} were estimated as − 8.3 kcal/mol and 1.22×10^6 M^{-1}, respectively. Interestingly, some amino acid residues of M^{pro} were commonly engaged with isoverbascoside and ritonavir such as Thr^{25}, Leu^{27}, His^{41}, Phe^{140}, Leu^{141}, Asn^{142}, Gly^{143}, Ser^{144}, Cys^{145}, His^{164}, Met^{165}, Glu^{166}, Pro^{168}, Gln^{189}, Thr^{190}, Ala^{191}, and Glu^{192}. Since isoverbascoside occupied a similar position at the active site of M^{pro} as occupied by a known inhibitor, i.e. ritonavir, and has a similar binding energy, it could act as a replace of ritonavir.

Docking to severe acute respiratory syndrome coronavirus 2 spike protein receptor-binding domain

The core of the S-protein's RBD comprises five-stranded antiparallel β-sheets (β1–4 and β7) with short interconnecting loops and helices. The receptor-binding motif of spike protein is formed by insertion of α4 and α5 helices and loops between β4 and β7 strands along with short β5 and β6 strands. Lan *et al.*[8] have reported that, during the analysis of the interface between the SARS-CoV-2 RBD and ACE2, 16 residues of RBD of spike protein interact with 20 residues of ACE2.[28] The residues of RBD of spike protein that interact with ACE-2 are Lys^{417}, Gly^{446}, Tyr^{449}, Tyr^{453}, Leu^{455}, Phe^{456}, Ala^{475}, Phe^{486}, Asn^{487}, Tyr^{489}, Gln^{493}, Gly^{496}, Gln^{498}, Thr^{500}, Asn^{501}, Gly^{502}, and Tyr^{505}.[28] The binding of all the studies ligand at the RBD of spike protein is described in details in Supplementary Data and shown in Supplementary Figure 4, Table 2, and Supplementary Table 6.

Among all compounds, the RBD – TM-10 complex exhibited the lowest binding energy revealing one carbon–hydrogen bond with Ser^{494} and one hydrophobic interaction with Tyr^{449} and eight conventional hydrogen bonds stabilized the complex (Arg^{403}, Glu^{406}, Tyr^{453}, Gln^{493}, Ser^{494}, Gly^{496} and Gln^{498}) [Table 2, Supplementary Table 6, and Supplementary Figure 4]. In addition, TM-10 formed a network of van der Waals' forces with Lys^{417}, Leu^{455}, Tyr^{495}, Phe^{497}, Asn^{501}, and Tyr^{505}. The docking energy and binding affinity of TM-10 toward RBD were estimated to be − 7.2 kcal/mol^{-1} and 1.91×10^5 M^{-1}, respectively.

The analyses of the interaction between *T. mollis* compounds and the RBD of SARS-CoV-2 spike protein suggested that all compounds can potentially bind at the interface of RBD-ACE2 but with different affinities. The binding energies of the compounds toward RBD were in the range of − 6.0 to − 7.2 kcal/mol. All the compounds interact with RBD's key amino acid residues such as Tyr^{505}, Asn^{501}, Thr^{500}, Gln^{498}, Gly^{496}, Gln^{493}, Tyr^{489}, Leu^{455}, Tyr^{453}, Tyr^{449}, and Lys^{417}. *Tecoma* compounds' interaction was primarily mediated through hydrogen bond(s) and hydrophobic interactions, except for TM-05. Thus, the isolated compounds hold the potential to be developed as an effective inhibitor of spike protein RBD of SARS-CoV-2.

For comparison, we also performed molecular docking of RBD with a control ligand namely azithromycin, and the results are presented in Table 2, Figure 3a, and Supplementary Table 5. The RBD–azithromycin complex was stabilized by three conventional hydrogen bonds with Arg^{403} and Tyr^{453} and eight hydrophobic interactions with Lys^{417}, Tyr^{453}, Leu^{455}, Phe^{456}, and Tyr^{495}. In addition, several amino acid residues of RBD such as Glu^{406}, Tyr^{449}, Gln^{493}, Ser^{494}, Gly^{496}, and Asn^{501} formed van der Waals' interaction. The binding energy and the corresponding binding affinity of azithromycin for RBD were determined as − 7.2 kcal/mol and 1.91 × 105 M^{-1}, respectively. It is noteworthy that isoverbascoside (TM-10) and azithromycin shared some common amino acid residue such as Arg^{403}, Lys^{417}, Tyr^{449}, Tyr^{453}, Leu^{455}, Gln^{493}, Ser^{494}, Tyr^{495}, Gly^{496}, and Asn^{501}. Since isoverbascoside (TM-10) was bound to RBD at a position occupied by azithromycin (control inhibitor) [Figure 3b and supplementary Table 6] and had a similar binding energy, it could act as a replace of azithromycin and thereby developed as a potential inhibitor of spike protein RBD.

Table 2: Molecular docking parameters for the interaction of compounds from *Tecoma mollis* with the receptor binding domain of severe acute respiratory syndrome coronavirus 2 spike protein

Compound	ΔG kcal mol^{-1}	Receptor amino acid
TM-01	−6.9	Arg^{403}, Tyr^{495}, Tyr^{505}, Gln^{493}, Gly^{496}, Asn^{501}
TM-02	−6.2	Tyr^{505}, Tyr^{453}, Ser^{494}, Gly^{496}, Gln^{498}, Asn^{501}
TM-03	−6.0	lys^{417}, Tyr^{505}, Arg^{403}, Glu^{406}, Gly^{496}, Glu^{484}
TM-04	−6.5	Gly^{496}, Tyr^{505}, Arg^{403}, Glu^{406}, Tyr^{505},
TM-05	−7.0	Arg^{403}, Tyr^{453}, Glu^{484}, Tyr^{505}
TM-06	−6.7	Gly^{496}, Tyr^{505}, Tyr^{453}, Leu^{492}, Gln^{493}
TM-07	−6.8	Ser^{494}, Tyr^{489}, Tyr^{505}, Phe^{490}, Gln^{493}, Gly^{496}, Gln^{498}
TM-08	−6.6	Arg^{403}, Glu^{406}, Lys^{417}, Tyr^{505}, Glu^{406}, Gln^{409}, Gly^{496}, Asn^{501}
TM-09	−6.9	Gly^{496}, Lys^{417}, Tyr^{505}, Glu^{406}, Glu^{484}, Phe^{490}, Asn^{501}
TM-10	−7.2	Ser^{494}, Tyr^{449}, Arg^{403}, Glu^{406}, Tyr^{453}, Gln^{493}, Gly^{496}, Gln^{498}
TM-11	−7.1	Lys^{417}, Leu^{455}, Tyr^{489}, Glu^{406}, Tyr^{453}, Glu^{484}, Gly^{496}
TM-12	−6.5	Tyr^{453}, Ser^{494}, Tyr^{505}, Gly^{496}, Gln^{498}, Thr^{500}, Asn^{501}
TM-13	−5.9	Tyr^{449}, Ser^{494}, Thr^{500}, Tyr^{505}
TM-14	−6.0	Tyr^{505}, Gly^{496}, Gln^{498}, Asn^{501},
TM-15	−6.5	Tyr^{495}, Ser^{494}, Gly^{496}, Gln^{498}, Asn^{501}
Azithromycin	−7.2	Arg^{403}, Lys^{417}, Tyr^{453}, Leu^{455}, Phe^{456}, Tyr^{495}

Tyr: Tyrosine; Glu: Glutamic acid; Gly: Glycine; Thr: Threonine; Ser: Serine; Phe: Phenylalanine; Leu: Leucine; Asn: Asparagine; Arg: Arginine; Gln: Glutamine; TM: *Tecoma mollis*

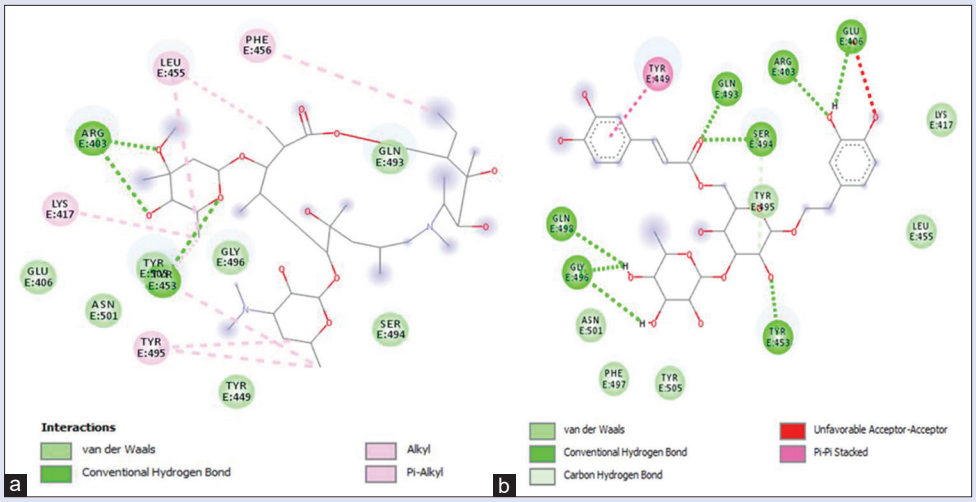

Figure 3: Two-dimensional ligand interaction diagram of (a) azithromycin and (b) isoverbascoside, with the receptor-binding domain of severe acute respiratory syndrome coronavirus 2 spike protein. Tyr: Tyrosine; Glu: Glutamic acid; Cys: Cysteine; Met: Methionine; Gly: Glycine; Val: Valine; Thr: Threonine; Ser: Serine; Phe: Phenylalanine; Pro: Proline; Leu: Leucine; Ala: Alanine; Asn: Asparagine; Ala: Alanine; His: Histidine; Arg: Arginine; Gln: Glutamine; Trp: Tryptophan

Molecular dynamic simulation

Root mean square deviation analysis

The dynamic nature of interaction and the stability of target proteins (M^{pro} and RBD) with their respective ligands (ritonavir, azithromycin, and isoverbascoside) were assessed by MD simulation under physiological conditions. The RMSD of a protein is a measure of its deviation from the initial structure and thus accounts for the stability of protein structure during simulation. The initial frames of M^{pro}–ritonavir and M^{pro}–isoverbascoside complexes were subjected to MD simulation for 100 ns [Figure 4a]. The RMSD of M^{pro}–ritonavir and M^{pro}–isoverbascoside complexes fluctuated within the acceptable limits throughout the simulation. The mean RMSD values of M^{pro} alone or in complex with ritonavir and isoverbascoside during 20–100 ns were estimated as 2.14 Å, 2.08 Å, and 1.86 Å, respectively. It should be noted that none of the fluctuations in RMSD were more than the acceptable limit of 2.00 Å, suggesting the formation of a stable M^{pro}–ritonavir and M^{pro}–isoverbascoside complexes. Similarly, the initial frames of RBD–azithromycin and RBD–isoverbascoside complexes were subjected to MD simulation for 100 ns [Figure 4b]. The RMSDs of RBD–azithromycin and RBD–isoverbascoside complexes were consistent and fluctuated within the acceptable limits throughout the simulation. The mean RMSD values of RBD alone or in complex with azithromycin and isoverbascoside during 20–100 ns were estimated as 2.28 Å, 2.83 Å, and 2.34 Å, respectively. It should be noted that none of the fluctuations in RMSD were more than the acceptable limit of 2.00 Å, suggesting the formation of a stable RBD–azithromycin and RBD–isoverbascoside complexes.

Root mean square fluctuation analysis

RMSF of a protein is a measure of local conformational changes in the side chains of a protein during MD simulation. The variation in RMSF of M^{pro} and RBD in the presence of their respective ligands, ritonavir, azithromycin, and isoverbascoside, was compared with the experimentally determined (during X-ray crystallography)

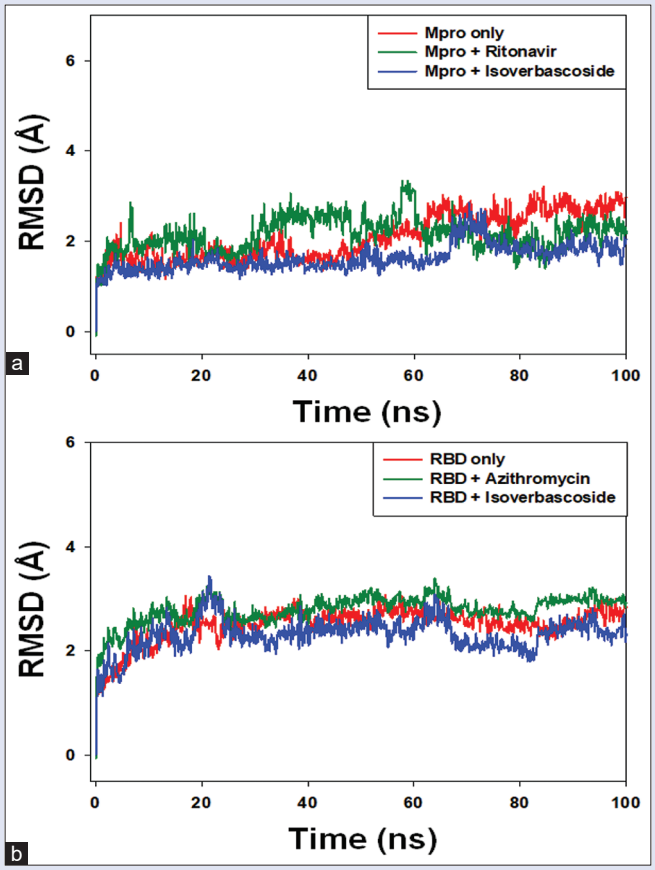

Figure 4: RMSD in the Cα-atoms of (a) main protease alone or in the presence of ritonavir and isoverbascoside and (b) spike protein receptor-binding domain alone or in the presence of azithromycin and isoverbascoside. RMSD: Root mean square deviation

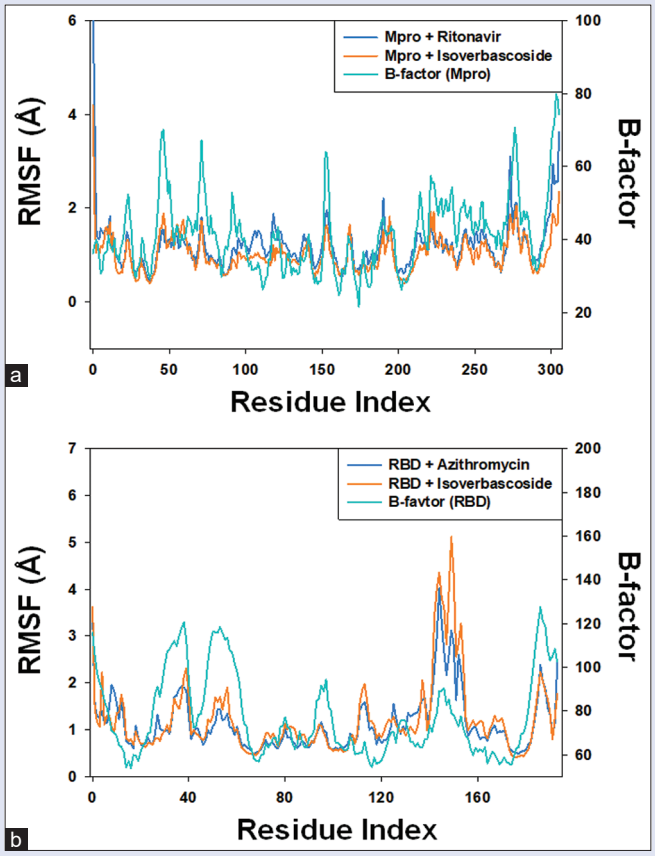

Figure 5: RMSF in the side chains of (**a**) main protease alone or in the presence of ritonavir and isoverbascoside and (b) spike protein receptor-binding domain alone or in the presence of azithromycin and isoverbascoside. For comparison, experimentally determined B-factors of main protease and receptor-binding domain are also indicated. RMSF: Root mean square fluctuation

B-factors [Figure 5]. The residues showing higher peaks correspond to loop regions or N- and C-terminal zones. The RMSF graphs of M^{pro}–ritonavir and M^{pro}–isoverbascoside complexes were overlapped with the B-factor of M^{pro} [Figure 5a]. Similarly, the RMSF graphs of RBD–azithromycin and RBD–isoverbascoside complexes were following the behavior of B-factor of RBD, within acceptable limits [Figure 5b]. It is evident that the RMSFs of M^{pro} and RBD did not deviate significantly in the presence of their respective ligands ritonavir, azithromycin, and isoverbascoside, assuring that the overall conformation of the protein remained conserved during MD simulation.

Analysis of radius of gyration and solvent accessible surface area

Rg and SASA of a ligand as a function of MD simulation measure the capacity of ligand to remain inside the binding pocket of protein. Moreover, Rg of a protein is an indication of the folded behavior of the protein during MD simulation. The variation in Rg of ligands ritonavir, azithromycin, and isoverbascoside bound with their respective protein targets M^{pro} and RBD as a function of MD simulation time is given in Figure 6a and 6b. The results show that Rg of M^{pro}–ritonavir and M^{pro}–isoverbascoside complexes varied within the acceptable limit in 20–100 ns MD simulation. Similarly, the Rg of RBD–azithromycin and RBD–isoverbascoside complex remained consistent during 20–100 ns simulation time. The average values of Rg for M^{pro}–ritonavir, M^{pro}–isoverbascoside, RBD–azithromycin, and RBD–isoverbascoside systems were 6.03, 5.64, 5.21, and 5.83 Å. All these results suggest that the ligands ritonavir, azithromycin, and isoverbascoside remained inside the binding cavity of their respective proteins M^{pro} and RBD in a stable conformation.

Total contacts formed between protein and ligand

The formation of a stable protein and ligand complex was established by determining the total number of contacts formed between them during MD simulation [Supplementary Figure 5]. The total number of contacts formed protein and ligand in M^{pro}–ritonavir, M^{pro}–isoverbascoside, RBD–azithromycin, and RBD-isoverbascoside systems varied between 3 and 14, 0 and 25, 0 and 10, and 0 and 14 respectively, with an average of 9, 16, 5, and 7 contacts, respectively.

Secondary structure analysis

The interaction between a ligand and protein often leads to changes in protein's secondary structural elements (SSEs). Thus, a check on the variation in SSE during simulation is critical to overview the establishment of a stable complex between target proteins and their respective ligands. The variation in total SSE (α-helix + β-sheet) of M^{pro} bound with ritonavir and isoverbascoside during MD simulation is presented in Supplementary Figure 6a and b. We found that the total SSEs of M^{pro} in complex with ritonavir and isoverbascoside were 40.54% (α-helix: 15.94% and β-sheets: 24.60%) and 38.73% (α-helix: 15.30% and β-sheets: 23.44%), respectively. Similarly, the variation in total SSE (α-helix + β-sheet) of RBD bound with azithromycin and isoverbascoside during MD simulation is presented in

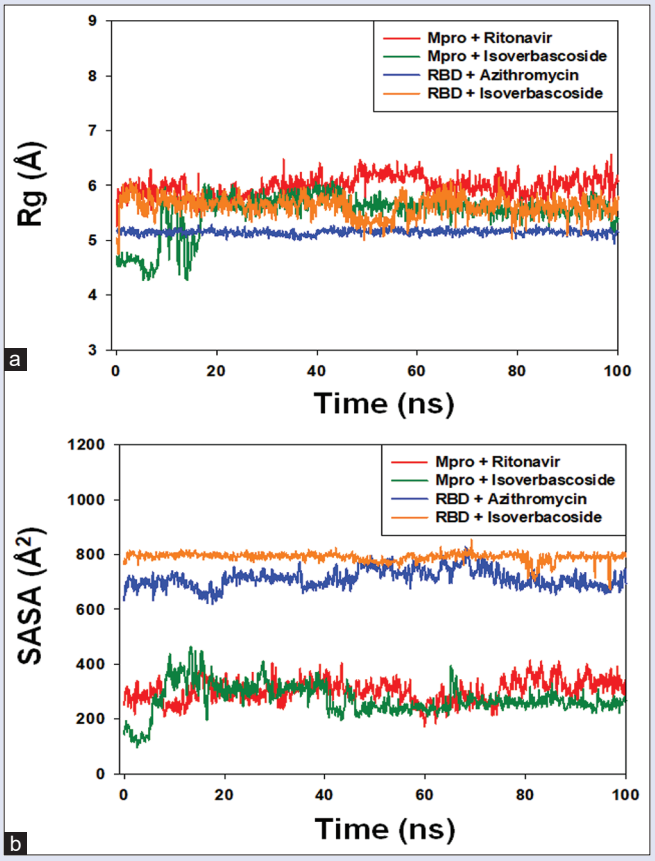

Figure 6: (a) Rg of M^{pro} and receptor-binding domain in the presence of their respective ligands, i.e. ritonavir, azithromycin, and isoverbascoside, and (b) SASA of M^{pro} and receptor-binding domain in the presence of their respective ligands, i.e. ritonavir, azithromycin, and isoverbascoside. Rg: Radius of gyration; M^{pro}: Main protease; SASA: Solvent accessible surface area

Supplementary Figure 6c and d. We found that the total SSEs of RBD in complex with azithromycin and isoverbascoside were 26.53% (α-helix: 3.61% and β-sheets: 22.93%) and 27.19% (α-helix: 4.66% and β-sheets: 22.52%), respectively. It should be noted that the SSEs of M^{pro} and RBD in combination with their respective ligands remained consistent throughout the simulation, suggesting a stable interaction between proteins and ligands.

Comparative structural evaluation of receptors interactions among the identified compounds

Phenylpropanoids and iridoids are diverse groups of natural products that are widely produced by various plant species.[30,31] These compounds possess diverse pharmacological properties, including their antiviral activities that have been reported in recent years.[14,15] Due to these prior results, we perform these molecular docking studies to investigate their potential inhibitory effects against both SARS-CoV-2 spike and M^{pro} enzymes. In the current study, all identified compounds had excellent binding stability with the catalytic residues of SARA-CoV-2 virus M^{pro} comparable to the currently used COVID-19 main protease inhibitors darunavir, lopinavir, remdesivir, and ritonavir [Table 1, Supplementary Table 5, and Figures 3, 4]. The strongest binding stability was observed with isoverbascoside (**10**) with binding energy − 8.8 kcal/mol, while the lesser binding stability was exhibited by the iridoid compound, ixoside (**15**), with binding energy − 7.3 kcal/mol [Table 1]. From Table 1, it is clear that the binding energies of most compounds are nearly similar to those of the currently used COVID-19 M^{pro} inhibitors, and it was concluded that the basic phenylpropanoid skeleton possesses higher binding stability than the phenolic glycosides followed by iridoids. Among the phenylpropanoids, it was apparent that glycosylation at OH-2' by apiose as in compound **3** dramatically reduces the binding stability and activity, while the glycosylation at OH-2' as in compound **9** by glucose has an unnoticeable effect compared with verbascoside (**1**). Furthermore, glycosylation of apiose at OH-3"" of the second glycosyl moiety forming the β-apiofuranosyl (1''' → 2')-β-glucopyranosid as in tecomolliside A (**5**) and tecomolliside B (**6**) has a small negative effect.

Moreover, acylation of caffeoyl moiety at OH-6', as in isoverbascoside (**10**), rather than OH-4' increase the binding stability and potentiate the activity compared with its isomer verbascoside (**1**). The acetylation of OH-6′ has negligible effect. Compounds with four phenolic hydroxyl groups exhibited stronger antioxidant activity than those with fewer numbers and methylation of free hydroxyl groups minimizes the activity, as in compound **13** and compound **14**. In summary, the order of binding strength and inhibition activity was as follows:

10 > 1, 2, 8, 9 > ritonavir, 4, 6, 12 > 5, 7 > lopinavir > darunavir, 11 > 13 > remdesivir > 3 > 14 >15.

In agreement with earlier reports for phenylpropanoids, verbascoside (**1**) and isoverbascoside (**10**) exhibited potent antiviral activity against different viruses, such as RSV, herpes simplex type 1, VSV, and influenza A virus H1N1 type.[14,15,32,33] These results suggest the potential effect of phenylpropanoids as novel inhibitors of SARS-CoV-2 with a better potency than that of the currently used protease inhibitors darunavir, lopinavir, remdesivir, and ritonavir [Table 1 and Figure 2].

Regarding S-protein inhibition activity, the compounds' molecular docking simulation exhibited lower binding stability and affinity to the RBD domain of the SARS-CoV-2 S-protein with high binding energy than to the M^{pro}. Similar to the outcome results from M^{pro} inhibition, isoverbascoside (**10**) exhibited the strongest binding stability with the lowest docking energy (−7.2 kcal/mol) compared to the S-protein inhibitor azithromycin [Table 2 and Figures 3, 4]. The order of binding stability strength was as follows:

10, azithromycin > 11 > 5 > 1, 9 > 7 > 6 > 8 > 4, 12, 15 > 3, 14 > 13.

Of the phenylpropanoid derivatives, the SAR of S-protein inhibition activity suggested the following: (i) compounds with caffeoyl moiety acylation at OH-6×, as seen in compound **10** and **11**, exhibited the highest binding stability compared to azithromycin; (ii) apiose glycosylation at OH-2 × reduce the activity, as seen in compound **3** and **4**; (iii) methylation of the phenolic hydroxyl groups reduce the binding stability and inhibitory action; (iv) in general, iridoids and phenyl glycosides exhibited lesser binding stability to S-protein than phenylpropanoid compounds.

CONCLUSION

COVID-19 is an infectious ailment caused by SARS-CoV-2 and led to a worldwide health emergency. At present, no specialized treatments are available for COVID-19 and finding a new drug that can interfere with the SARS-CoV-2 replication/transcription or its entrance into the target cells, is urgently needed. The feasibility of computational tools such as molecular docking, high-throughput virtual screening, molecular dynamic simulation, and free energy calculation has been assured in the past for identifying inhibitors from a collection of ligand databases.

In the current study, a phytochemical investigation of the *T. mollis* (Humb and Bonpl.) heartwood afforded isolation of 12 phenylpropanoids, two phenolic glycosides, and one iridoid, which were first reported from the plant heartwood – investigating the anti-SARS-CoV-2 activity of the isolated compounds **1–15** by employing computational approaches

to screen their activity in targeting the proteins of SARS-CoV-2 for identification of antiviral therapeutics. The study focuses on two target proteins essential in the life cycle of SARS-CoV-2, S-protein RBD, and M^{pro}. Molecular docking was performed to determine the compounds' feasibility as potential inhibitors of these target viral proteins. Further, molecular dynamic simulation was performed to confirm the stability of protein–ligand complexes.

The molecular docking simulation showed that isoverbascoside (**10**) exhibited strong inhibitory action for SARS-CoV-2 M^{pro} and S-protein RBD as compared to the currently used inhibitors and is considered a promising a dual SARS-CoV-2 M^{pro} and S-protein inhibitor. Isoverbascoside is often named as isoacteoside; it is widely distributed in the plant kingdom and has extraordinary pharmacological and therapeutic activities, e.g. antioxidant, anti-inflammatory, antinociceptive, antihepatotoxic, and antiviral activities.[34] Thus, based on the findings of this study, more *in vitro* and *in vivo* studies of the anti-SARS-CoV-2 activity of phenylpropanoids, in general, and isoverbascoside, in particular, are necessary, as they could assist in discovering drugs to target the current SARS-CoV-2 pandemic. In the meanwhile, a wet laboratory *in vitro* assay is carried out to confirm the effectiveness of isoverbascoside as M^{pro} and S-protein RBD inhibitor.

Financial support and sponsorship

This work was funded by the Deanship of Scientific Research at Princess Nourah bint Abdulrahman University, through the Research Groups Program Grant no. (RGP-1440-0014)(2).

Conflicts of interest

There are no conflicts of interest.

REFERENCES

1. Astuti I, Ysrafil Y. Severe Acute Respiratory Syndrome Coronavirus 2 (SARS-CoV-2): An overview of viral structure and host response. Diabetes Metab Syndr 2020;14:407-12.
2. Pal M, Berhanu G, Desalegn C, Kandi V. Severe acute respiratory syndrome coronavirus-2 (SARS-CoV-2): An update. Cureus 2020;12:e7423.
3. Satarker S, Nampoothiri M. Structural proteins in severe acute respiratory syndrome coronavirus-2. Arch Med Res 2020;51:482-91.
4. Duan L, Zheng Q, Zhang H, Niu Y, Lou Y, Wang H. The SARS-CoV-2 spike glycoprotein biosynthesis, structure, function, and antigenicity: Implications for the design of spike-based vaccine immunogens. Front Immunol 2020;11:576622.
5. Yang J, Petitjean SJL, Koehler M, Zhang Q, Dumitru AC, Chen W, *et al.* Molecular interaction and inhibition of SARS-CoV-2 binding to the ACE2 receptor. Nat Commun 2020;11:4541.
6. Yang JS, Chiang JH, Tsai SC, Hsu YM, Bau DT, Lee KH, *et al. In silico de novo* curcuminoid derivatives from the compound library of natural products research laboratories inhibit COVID-19 3CLpro activity. Nat Prod Commun 2020;15:1-15.
7. Zhang L, Lin D, Sun X, Curth U, Drosten C, Sauerhering L, *et al.* Crystal structure of SARS-CoV-2 main protease provides a basis for design of improved α-ketoamide inhibitors. Science 2020;368:409-12.
8. Lan J, Ge J, Yu J, Shan S, Zhou H, Fan S, *et al.* Structure of the SARS-CoV-2 spike receptor-binding domain bound to the ACE2 receptor. Nature 2020;581:215-20.
9. World Health Organization, COVID-19 Studies from the World Health Organization Database. Available from: http://www.https://clinicaltrials.gov/ct2/who_table/. [Last accessed on 2020 Dec 12].
10. El-Emary NA, Khalifa AA, Backheet EY, Abdel-Mageed WM. Macro- and micromorphology of the leaf, stem and stem bark of *Tecoma mollis* Humb. and Bonpl. cultivated in Egypt. Bull Pharm Sci Assiut Univ 2001;24:173-99.
11. El-Emary NA, Khalifa AA, Backheet EY, Abdel-Mageed WM. Phytochemical and biological studies on the leaves of *Tecoma mollis* Humb. and Bonpl. cultivated in Egypt. Bull Pharm Sci Assiut Univ 2002;25:207-28.
12. Abdel-Mageed WM, Backheet EY, Khalifa AA, Ibraheim ZZ, Ross SA. Antiparasitic antioxidant phenylpropanoids and iridoid glycosides from *Tecoma mollis*. Fitoterapia 2012;83:500-7.
13. Abdel-Mageed WM, Al-Wahaibi LH, Backheet EY, El-Gamal AA, Gouda YG, Basudan OA, *et al.* New phenolic glycosides with cyclooxygenase inhibition from the roots of *Tecoma mollis*. Phytochem Lett 2017;21:98-103.
14. Kernan MR, Amarquaye A, Chen JL, Chan J, Sesin DF, Parkinson N, *et al.* Antiviral phenylpropanoid glycosides from the medicinal plant *Markhamia lutea*. J Nat Prod 1998;61:564-70.
15. Bermejo P, Abad MJ, Díaz AM, Fernández L, De Santos J, Sanchez S, *et al.* Antiviral activity of seven iridoids, three saikosaponins and one phenylpropanoid glycoside extracted from *Bupleurum rigidum* and *Scrophularia scorodonia*. Planta Med 2002;68:106-10.
16. Chen YP, Tan DP, Zeng Q, Wang Y, Yan QX, Zeng LJ. Chemical constituents from leaves of *Acanthus ilicifolius* and their anti-influenza virus activities. Zhong Yao Cai 2015;38:527-30.
17. de Oliveira OV, Rocha GB, Paluch AS, Costa LT. Repurposing approved drugs as inhibitors of SARS-CoV-2 S-protein from molecular modeling and virtual screening. J Biomol Struct Dyn 2021;39:3924-33.
18. Du X, Zuo X, Meng F, Han C, Ouyang W, Han Y, *et al.* Direct inhibitory effect on viral entry of influenza A and SARS-CoV-2 viruses by azithromycin. Cell Prolif 2021;54:e12953.
19. Cao B, Wang Y, Wen D, Liu W, Wang J, Fan G, *et al.* A trial of Lopinavir-Ritonavir in adults hospitalized with severe Covid-19. N Engl J Med 2020;382:1787-99.
20. Ghosh R, Chakraborty A, Biswas A, Chowdhuri S. Identification of polyphenols from *Broussonetia papyrifera* as SARS CoV-2 main protease inhibitors using *in silico* docking and molecular dynamics simulation approaches. J Biomol Struct Dyn 2020 ;1-14.
21. Trott O, Olson AJ. AutoDock Vina: improving the speed and accuracy of docking with a new scoring function, efficient optimization, and multithreading. J Comput Chem 2010;31:455-61.
22. Duru CE, Umar HIU, Duru IA, Enenebeaku UE, Ngozi-Olehi LC, Enyoh CE. Blocking the interactions between human ACE2 and coronavirus spike glycoprotein by selected drugs: a computational perspective. Environ Anal Health Toxicol 2021;36:e2021010-0.
23. Al-Shabib NA, Khan JM, Malik A, Alsenaidy MA, Rehman MT, AlAjmi MF, *et al.* Molecular insight into binding behavior of polyphenol (rutin) with beta lactoglobulin: Spectroscopic, molecular docking and MD simulation studies. J Mol Liq 2018;269:511-20.
24. AlAjmi MF, Rehman MT, Hussain A, Rather GM. Pharmacoinformatics approach for the identification of Polo-like kinase-1 inhibitors from natural sources as anti-cancer agents. Int J Biol Macromol 2018;116:173-81.
25. Rehman MT, Shamsi H, Khan AU. Insight into the binding mechanism of imipenem to human serum albumin by spectroscopic and computational approaches. Mol Pharm 2014;11:1785-97.
26. Rehman MT, Ahmed S, Khan AU. Interaction of meropenem with 'N' and 'B' isoforms of human serum albumin: A spectroscopic and molecular docking study. J Biomol Struct Dyn 2016;34:1849-64.
27. Branka AC. Nose-hoover chain method for nonequilibrium molecular dynamics simulation. Phys Rev E Stat Phys Plasmas Fluids Relat Interdiscip Topics 2000;61:4769-73.
28. Martyna GJ, Tobias DJ, Klein ML. Constant pressure molecular dynamics algorithms. J Chem Phys 1994;101:4177-89.
29. Jin Z, Du X, Xu Y, Deng Y, Liu M, Zhao Y, *et al.* Structure of M^{pro} from SARS-CoV-2 and discovery of its inhibitors. Nature 2020;582:289-93.
30. Kurkin VA. Phenylpropanoids from medicinal plants: Distribution, classification, structural analysis and biological activity. Chem Nat Compd 2003;39:123-53.
31. Dinda B. Occurrence and distribution of iridoids. In: Pharmacology and Applications of Naturally Occurring Iridoids. Ch. 2. Cham, Basel, Switzerland: Springer; 2019. p. 17-82.
32. Song X, He J, Xu H, Hu XP, Wu XL, Wu HQ, *et al.* The antiviral effects of acteoside and the underlying IFN-γ-inducing action. Food Funct 2016;7:3017-30.
33. Hu XP, Shao MM, Song X, Wu XL, Qi L, Zheng K, *et al.* Anti-influenza virus effects of crude phenylethanoid glycosides isolated from ligustrum purpurascens via inducing endogenous interferon-γ. J Ethnopharmacol 2016;179:128-36.
34. Li L, Tsao R, Liu Z, Liu S, Yang R, Young JC, *et al.* Isolation and purification of acteoside and isoacteoside from *Plantago psyllium* L. by high-speed counter-current chromatography. J Chromatogr A 2005;1063:161-9.